J Mater Sci: Mater Electron (2015) 26:4840–4847
DOI 10.1007/s10854-015-2991-6

CrossMark

Surface evolution of sputtered $Cu(In,Ga)Se_2$ thin films under various annealing temperatures

Jun-feng Han[1,4] · Liang-qi Ouyang[2] · Da-ming Zhuang[2] · Ming Zhao[2] · Cheng Liao[2] · Jiang Liu[2] · Limei Cha[3,4] · M.-P. Besland[4]

Received: 31 January 2015 / Accepted: 21 March 2015 / Published online: 27 March 2015
© Springer Science+Business Media New York 2015

Abstract In this work, copper indium gallium selenide (CIGS) thin films were prepared by sputtering CIGS quaternary target and subsequent annealing under Se atmosphere in the 240–550 °C range. X-ray diffraction (XRD), Grazing incidence x-ray diffraction (GIXRD), Raman spectroscopy and X-ray photoelectron spectroscopy (XPS) were performed to investigate the crystalline structures and chemical compositions of the CIGS thin films. According to XRD, GIXRD and Raman analyses, the CIGS phase was splitted into CuSe phase and In_4Se_3 phase at the very surface when CIGS was annealed at 240 and 270 °C. In addition, XRD patterns indicated a grain size growth with increasing temperature. XPS analyses contributed more information on the film surface chemistry. Indeed, O 1 s and Na 1 s signals were observed at the film surface above 380 °C, and were even increased from 450 to 550 °C. Simultaneously, the surface appeared to exhibit a Cu and Ga poor surface chemical composition. The strong correlation between O, Na and Cu atomic contents in the CIGS surface were discussed in the paper.

✉ Jun-feng Han
pkuhjf@bit.edu.cn; pkuhjf@gmail.com

[1] Present Address: School of Physics, Beijing Institute of Technology, Beijing 100081, China

[2] School of Materials Science and Engineering, Tsinghua University, Beijing 100084, China

[3] College of Materials Science and Engineering, Hunan University, Changsha 410082, China

[4] Institut des Matériaux Jean Rouxel (IMN), Université de Nantes, UMR CNRS 6502, 44322 Nantes, France

1 Introduction

Chalcopyrite semiconductors are promising materials for high efficiency and low cost thin film solar cells [1]. Copper indium gallium selenide (CIGS) based polycrystalline semiconductor has been widely used for thin film solar cells and becomes one of the most popular materials in the recent years [2, 3]. The CIGS device efficiency has recently reached 20.8 % at laboratory scale [4]. Different promising synthesis routes for CIGS absorber layer growth have been investigated, such as co-evaporation [5], selenization of metallic precursor [6], nano-ink printing [7] and electrical deposition [8].

Co-evaporation method is well known to prepare high quality CIGS absorbers. However, the success of this technique strongly depends on an accurate control of the individual elemental fluxes during the deposition, which is a challenge for large-scale mass manufacture [9, 10]. Post-selenization of metallic precursors is another recognized method to prepare high quality film over large areas. The Cu–In–Ga precursors are typically prepared by sputtering metal and alloy targets (such as In and CuGa targets). However, the process of post-selenization involves complicated phase formations, which easily leads to Ga accumulation at the back side of films [11, 12] and consequently inhomogeneous absorption layers. One simple route is to deposit the absorption layer by sputtering a quaternary CIGS target and subsequently annealing the films [13]. Such method allows fabricating homogeneous chalcopyrite films leading to high efficiency solar cells in the 16–20 % range [14]. Up to now, all developed processes have needed an annealing step. Consequently, deeper knowledges on material evolution during the annealing process of film are crucial to optimize the film preparation process and its ultimate properties.

As-sputtered CIGS films are considered exhibiting a chalcopyrite structure, which needs a post-deposition annealing step to improve its crystalline quality [15, 16]. Some research works have recently reported on the properties of sputtered CIGS films and their device performances [17, 18]. However, few works report on the detail study of CIGS film evolutions during the annealing process, especially the crystalline phases and chemical composition variations. Therefore, to gain more information on material processing, it is necessary to investigate the surfaces and bulks at various annealing temperatures in detail.

In this paper, we reported on CIGS film deposition by a quaternary target sputtering and subsequent the annealing process from 240 to 550 °C under a Se-containing atmosphere. Our aim was to investigate the film surface modifications during the annealing processes. The crystal structures and chemical compositions of thin films were characterized by X-ray diffraction (XRD), grazing incidence x-ray diffraction (GIXRD), Raman spectroscopy and X-ray photoelectron spectroscopy (XPS). The relationships between film surface modifications and annealing temperature variation were also discussed in the present paper.

2 Experimental

2.1 Film deposition

In the first step, the CIGS precursor films were deposited by RF magnetron sputtering a CIGS quaternary target under an Argon pressure of 0.7 Pa. During the deposition, the substrate temperature was maintained at 200 °C by a PID controller. Thin films were deposited on Mo-coated soda-lime glass (SLG) substrates. The average thickness of ~1 μm was measured by profilometer. The sputtering parameters have been optimized and reported in previous works [15, 17].

In the second step, as-deposited films were annealed in a tubular furnace under 5×10^4 Pa Ar pressure. Selenium (Se) vapour was introduced into the chamber from a Se source located at the bottom of furnace as shown in Fig. 1. The Se amount was chosen to create a Se over-pressure and thus Se loss would be compensated during the annealing step. All CIGS samples were submitted to a 30 min annealing and various annealing temperatures are: 240, 270, 310, 340, 380, 410, 450, 480, 510 and 550 °C. On the basis of previous studies [19], the annealing temperatures values were selected in order to investigate the surface modification and crystallization process of CIGS films.

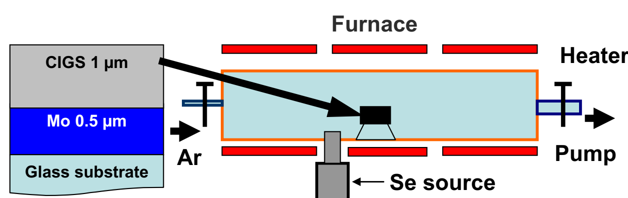

Fig. 1 Schematic of the annealing system: Se source at the *bottom part* in order to generate Se vapour during annealing

2.2 Characterization

The crystalline phases of thin films were checked by XRD using RICOH-DX12 with Cu Kα (λ = 1.5418 Å) radiation in θ–2θ mode. The surface crystalline was investigated by GIXRD using a Siemens D5000 "PSD" with Cu Kα radiation (λ = 1.5418 Å) at 1° incidence angle. The Raman spectra were recorded in back scattering geometry at room temperature, using a T64000 Jovin Yvon spectrometer with the He–Ne 633 nm laser line. Related references were used to identify Raman peaks [20–22]. XPS studies were performed using a Kratos Nova spectrometer with a monochromatized Al anode X-ray source (hν = 1486.6 eV) equipped with Ar ion sputtering gun. Sputtering was performed with 2 kV Ar ions leading to a typical sputtering rate of 4 nm/min. Survey scans and relevant core levels were recorded: Cu 2p, In 3d, Ga 2p, Se 3d and Na 1 s. Atomic elemental contents were further extracted from peaks area taking into account sensitivity factors.

3 Results and discussion

3.1 Phase evolutions versus annealing temperatures

3.1.1 XRD analyses of CIGS films versus annealing temperature

XRD patterns of annealed CIGS films under Se excess are displayed in Fig. 2a. In all patterns, the diffraction peak of Mo glass coating is recorded at 40.4°. Since XRD patterns of the annealed CIGS films above 380 °C are very similar, only some of them are selected and shown in Fig. 2. Starting from the bottom of Fig. 2a, as-deposited CIGS film exhibits a single diffraction peak at 27.0°, which is associated to (112) plane of CIGS phase ($Cu(In,Ga)Se_2$, JCPDS file 35-1102). According to JCPDS file, which characterizes a randomly oriented phase, we can assume that the as-deposited CIGS film exhibits a strongly preferential plane as (112). When annealed at 240 °C, two new diffraction peaks appear at 29.2° and 31.2° on the pattern. The former one can be related to (040/140) planes of In_4Se_3 phase (JCPDS file 51-0808), while the latter one is related to (006) plane of CuSe phase (JCPDS file 65-3562). As increasing the temperature further to 270 °C, the diffraction peak of In_4Se_3 at 29.2° disappears completely.

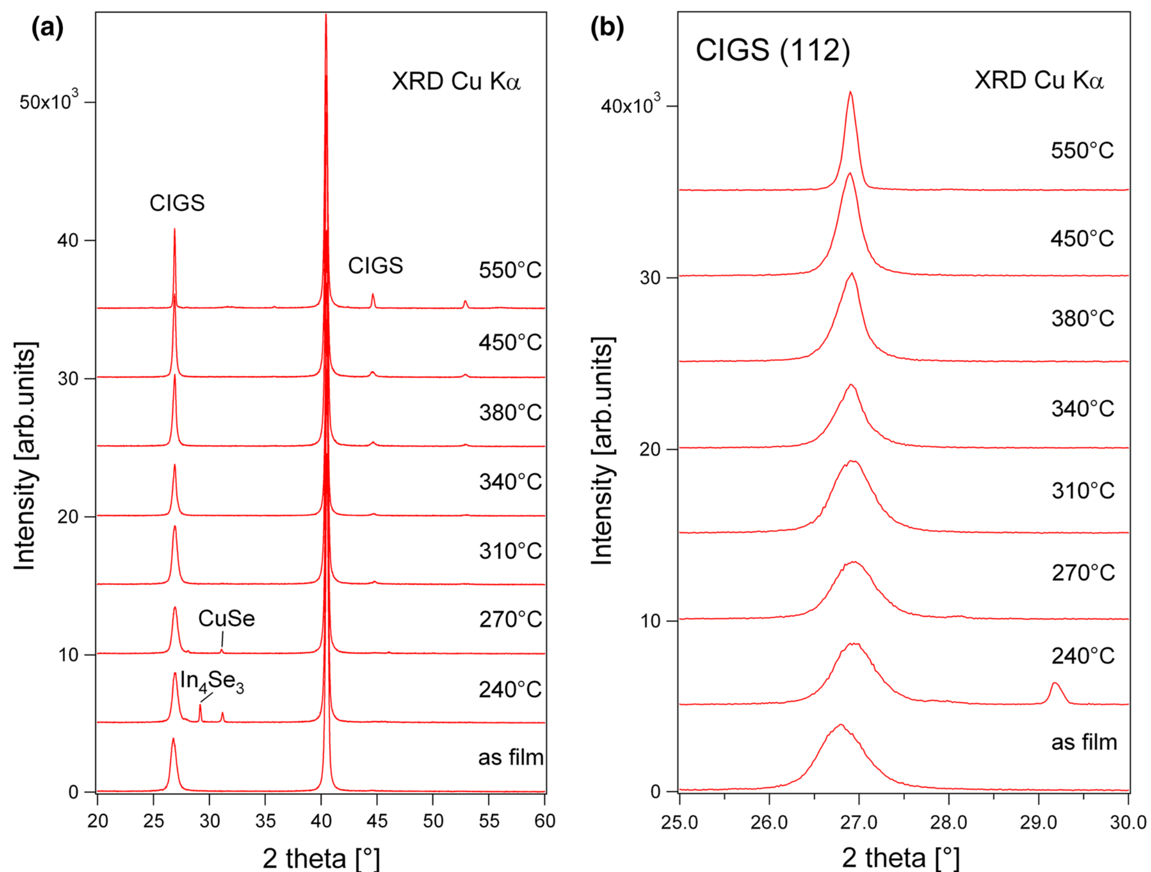

Fig. 2 XRD patterns in θ–2θ mode for CIGS films, as-deposited and the ones after 30 min annealing at temperatures ranging from 240 to 550 °C: **a** for the entire 2θ ranging from 20° to 60°; **b** selected 2θ range from 25° to 30°

Simultaneously, the intensity of the CuSe peak at 31.2° is decreasing significantly and completely disappeared at 310 °C. Instead, a new diffraction peak is observed at 44.8° and can be associated to (204/220) diffraction plane of CIGS phase (JCPDS file 35-1102). With increasing temperature from 310 to 550 °C, the intensity of (204/220) peak is increasing progressively. As a conclusion, starting from a preferentially oriented crystalline structure of (112) plane, the last annealing step at 550 °C leads to a more randomly crystallized CIGS film, exhibiting a XRD pattern with diffraction peak intensities closer to the JCPS file (35-1102).

To complete the study, XRD patterns in the 25°–30° range are shown in Fig. 2b and allow to follow the evolution of the full width at half maximum (FWHM) value of (112) diffraction peak versus annealing temperatures. It appears that the peak width decreases from an initial value of 0.54°, for as-deposited film, to a final value of 0.22°, after annealing at 550 °C. Using the Scherrer formula, an average grain size can be roughly calculated from FWHM of XRD diffraction peak. Clearly, the crystallite size is increasing from 16 to more than 40 nm after annealing at 550 °C. Theses XRD analyses highlight the enhancement of crystallization process during the annealing step of sputtered CIGS films. After 30 min annealing at 550 °C, the CIGS sputtered films exhibit a polycrystalline and randomly oriented structure with increased grain size in the 40–50 nm range.

3.1.2 *GIXRD analyses of CIGS films versus annealing temperature*

GIXRD analyses were performed to investigate the crystalline characters of thin films at their extreme surface. The recorded diffraction patterns are displayed in Fig. 3. Again, since GIXRD patterns recorded for films annealed above 380 °C are very similar, only the selected patterns are shown in Fig. 3. Since the incident angle is 1°, the detected depth is estimated to be only 100 nm. Consequently, no Mo diffraction peak can be observed in all these XRD patterns.

At the bottom of Fig. 3, the XRD pattern of as-deposited CIGS film exhibits only one diffraction peak at 27.0°, corresponding to the (112) diffraction plane of CIGS phase

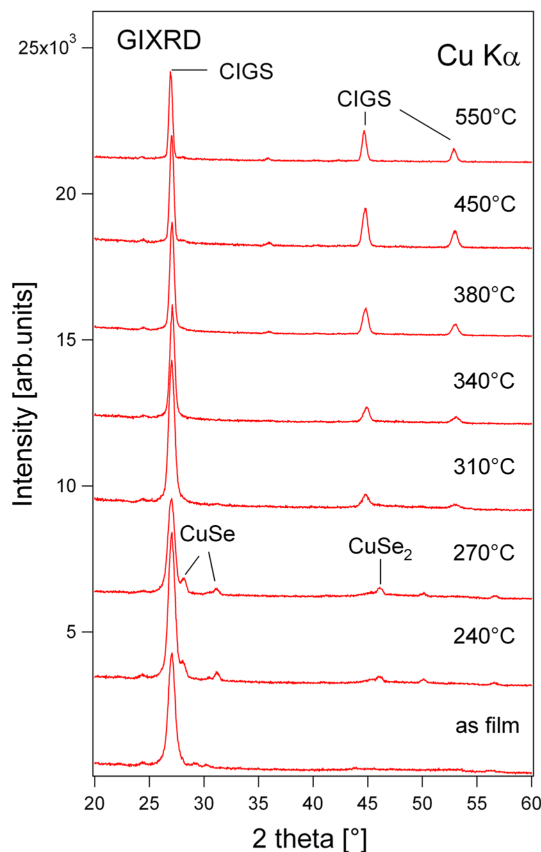

Fig. 3 GIXRD patterns in θ–2θ mode for CIGS films, as-deposited film and the ones after 30 min annealing at temperatures ranging from 240 to 550 °C

($Cu(In,Ga)Se_2$, JCPDS file no 35-1102). For annealing at 240 °C, three new diffraction peaks are appearing at 28.0°, 31.2° and 46.1°. The first two peaks are respectively related to (102) and (006) diffraction planes of CuSe phase (JCPDS file no 65-3562). The last one is related to (211) diffraction plane of $CuSe_2$ phase ($CuSe_2$, JCPDS file no 19-0400). Nevertheless, no diffraction peak associated to In_4Se_3 phase can be observed in that pattern series. It means that no In_4Se_3 phase is detected in the first 100 nm of the annealed films. Compared with previous XRD results, we can suppose that, in this temperature range, CIGS films are constituted of In_4Se_3, CuSe and $CuSe_2$ phases. CuSe and $CuSe_2$ phases exists at the film surface, while In_4Se_3 phase may be located below the film surface within the bulk of the thin film. Consequently, only CuSe and $CuSe_2$ phases can be detected by GIXRD. For the film annealing at 270 °C, the grazing XRD pattern exhibits diffraction peaks related to CIGS phase (JCPDS file no 35-1102), as well as CuSe and $CuSe_2$ phases (JCPDS file no 65-3562 and no 19-0400, respectively), very similar to the one annealing at 240 °C. For the sample annealed at 310 °C, the diffraction peaks at 28.0°, 31.2° and 46.1°, associated to CuSe and $CuSe_2$ phases are completely disappeared. Simultaneously, a new diffraction peak is observed at 44.8° and corresponds to (204/220) diffraction plane of CIGS phase (JCPDS file no 35-1102). As increasing annealing temperature from 310 to 550 °C, the intensity of (204/220) peak is increasing largely, as observed previously by XRD.

3.1.3 *Raman spectra of of CIGS films versus annealing temperature*

Figure 4 displays Raman spectra recorded at room temperature from the as-deposited and absorber films after 30 min annealing at the temperature between 240 and 550 °C. All the films were deposited under Se excess atmosphere. Raman spectra of selected films are shown in Fig. 4, since the spectra are very similar above 380 °C. Raman spectroscopy is a surface technology with a detection depth depending on the laser wavelength, which has been estimated to be 100–200 nm in this work. Starting from the bottom of Fig. 4, as-deposited CIGS film spectrum exhibits a broad frequency at 174 cm^{-1} attributed to A1 mode of CIGS compound. For sample prepared at 240 °C, the frequency of A1 mode becomes broader with a shoulder appearing at 158 cm^{-1}. The shoulder could be

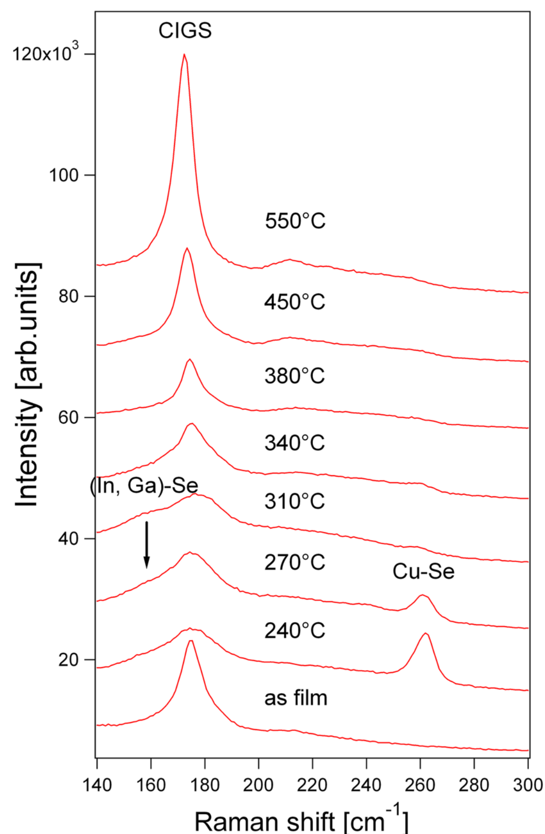

Fig. 4 Raman spectra for CIGS films, as-deposited film and the ones after 30 min annealing at temperatures ranging from 240 to 550 °C

associated to In or Ga selenide (In,Ga)Se according to the literature [20–22]. In addition, a new mode is observed at 260 cm^{-1}, which can be related to Cu–Se compounds, like CuSe or Cu_2Se. After annealing at 270 °C, the intensity of Cu–Se mode (260 cm^{-1}) starts to decrease and disappears completely after annealing at 310 °C. Simultaneously, the frequency at 174 cm^{-1} becomes narrower with some additional weak shoulders at lower frequency. As the temperature is increasing up to 380 °C, the weak shoulder below 174 cm^{-1} disappears and a new frequency related to B1 mode of CIGS appears at 212 cm^{-1}. Above 380 °C, higher annealing temperatures enhance the increase of peak intensity and decrease of the FWHM value of main frequency at 174 cm^{-1}.

Considering results in the present study, we may develop some comments on chemical phases of sputtered and as-deposited CIGS films versus annealing under Se atmosphere. As a first step, between 240 and 270 °C, according to XRD, GIXRD and Raman analyses, the film surface is covered by $CuSe_x$ phases. A characteristic solid–vapor reaction may take place in the film surface, similar to the model described previously [23, 24]. Initially, gaseous Se_8 molecules can be absorbed on the film surface and react with Cu atoms, leading to the formation of isolated nucleation centers. In the second stage, more adsorbed Se_8 molecules and Cu atoms may diffuse into the early formed nucleation centers, which promote a local preferential growth of $CuSe_x$ phases at the surface. As a result, the CIGS phase splits near the film surface, i.e. $CuSe_x$ show up near the film surface, while a Cu poor phase, $(In,Ga)_4Se_3$ phase, is formed just below the film surface.

3.2 Chemical composition near the surface versus annealing temperature

3.2.1 XPS surface analyses of CIGS films

Chemical composition of CIGS thin film surface was characterized by XPS. Starting from atomic elemental contents extracted from peaks area, significant atomic ratios have been calculated to follow surface chemical evolution of CIGS films versus annealing temperature. Figure 5 displays the evolution of chemical composition at film surfaces for 30 min annealing under Se excess atmosphere at temperatures from 240 to 550 °C. Significant atomic ratios are considered, i.e. Cu/(In + Ga) and Ga/(In + Ga) atomic ratios, and displayed in Fig. 5a, b, respectively. In addition, the evolutions of sodium and oxygen contents are also considered (Fig. 5c, d, respectively). In Fig. 5a, the initial Cu/(In + Ga) ratio at the film surface is close to 1.0. For annealing below 310 °C, Cu/(In + Ga) ratio increase progressively up to 1.2. Then the ratio is decreasing with increasing annealing temperature. Finally, for CIGS film annealed at 550 °C, Cu/(In + Ga) ratio at the film surface is only 0.45, which is far below its initial value of 1. In Fig. 5b, the initial Ga/(In + Ga) ratio in as-deposited CIGS film is 0.37. For annealing below 310 °C, Ga/(In + Ga) ratio remains in the range of 0.3–0.35, i.e. very close to stoichiometric chemical composition of as-deposited CIGS sputtered films. Afterward, it decreases down to $\sim$0.2 for annealing temperature between 340 and 450 °C. For annealing above 450 °C, Ga/(In + Ga) ratio decreases further down to $\sim$0.15. While comparing this value to the initial one of 0.37, we may conclude that a Ga poor component is formed after annealing step at temperature above 450 °C. As shown in Fig. 5c, d, no obvious Na and O signals are initially detected at the film surface and after annealing step below 380 °C. For the film annealed at 380 °C, Na and O signals with significant atomic content are recorded. Furthermore, a fast and huge increase of Na and O contents are observed with increasing annealing temperatures ranging from 380 to 450 °C. After annealing at 450 °C, the Na content reaches 30 % atomic percent, while O content increases up to 10 %. Above 450 °C, Na and O contents remain around 30 and 10 % on the film surfaces, respectively.

3.2.2 XPS depth profile of annealed CIGS thin films

To investigate the distribution of Cu, Ga, Na and O atomic contents from the surface towards the bulk, CIGS samples annealed at various temperatures, namely 380, 410, 450 and 550 °C were selected. In order to gain some insights into both the film and bulk chemical compositions and their evolutions versus annealing temperature, in situ Ar ion etching under 2-kV-mode were used in XPS experiments. Sputtering step of 1 min duration were performed and the sputtering rate was estimated to be in the 4 nm/min range. Therefore, the analyzed depth was approximately 10 nm for CIGS films annealed at 380 and 410 °C and close to 30 nm from the film surface for the two higher temperature values, 450 and 550 °C. Similarly to the previous section, the atomic contents, Cu/(In + Ga) and Ga/(In + Ga) atomic ratios were determined. The evolution of those two ratios and Na and O contents are shown in Fig. 6a–d. As displayed in Fig. 6a, Cu/(In + Ga) ratio is increasing progressively with the film depth. For annealing at 380 and 410 °C, the ratio increases slowly from 0.65 at the film surface to 0.8 at the end of sputtering (10 nm in depth). After annealing at 450 °C, the initial Cu/(In + Ga) ratio is lower than 0.6 and it increases to nearly 0.8 in the bulk, i.e. at 30 nm in depth from the film surface. In the case of annealing at 550 °C, the Cu/(In + Ga) ratio starts from a lower level of 0.45 and reaches finally 0.65 in the deeper analyzed area. Therefore, we may assume that a Cu poor layer is formed at the surface vicinity during the annealing

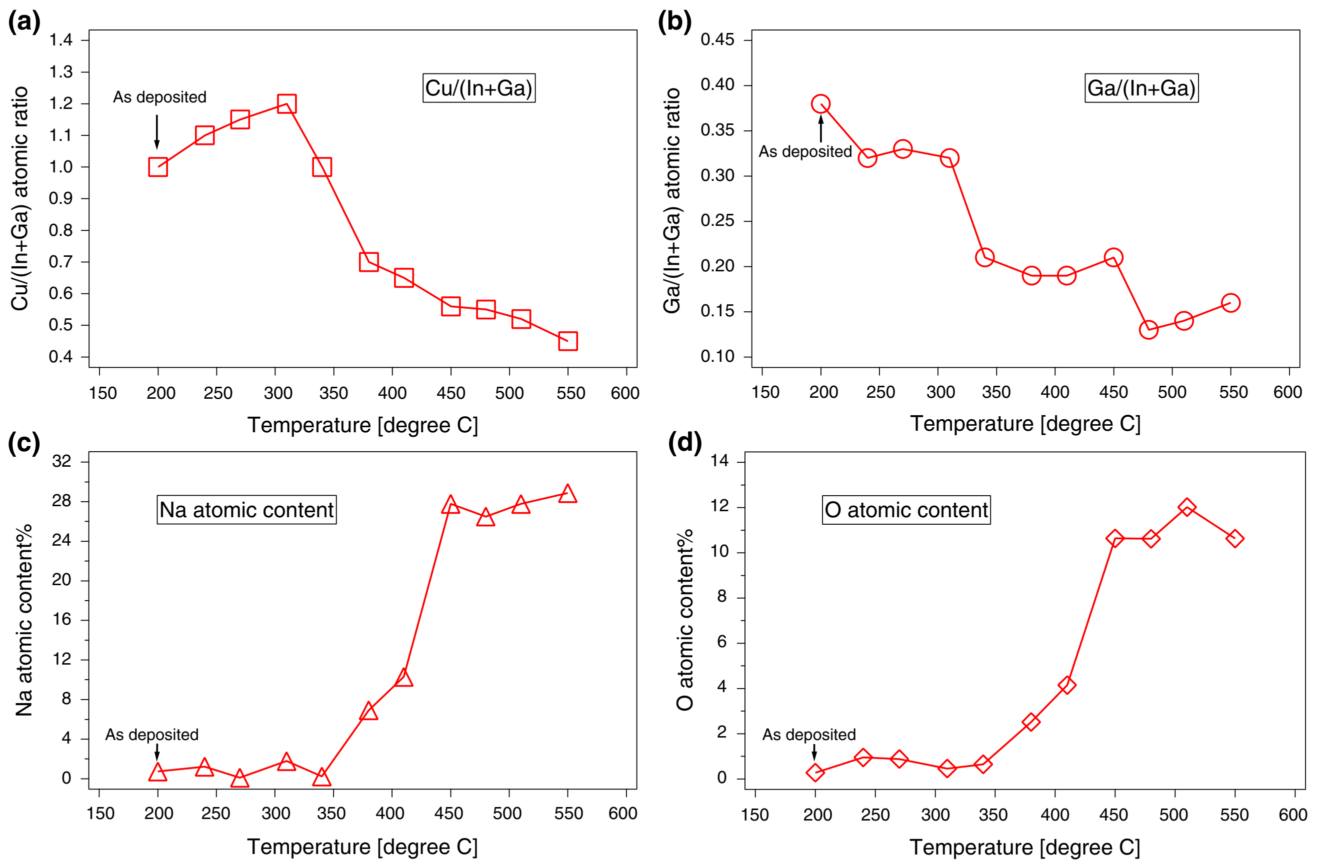

Fig. 5 Variation of atomic ratios **a** Cu/(In + Ga) and **b** Ga/(In + Ga) obtained from XPS core levels analyses (Cu 2p, In 3d and Ga 2p) at the surface of CIGS films, the film as deposited and the ones after 30 min. annealing at temperatures from 240 to 550 °C, (**c**, **d**) are the variation of Na and O atomic content versus annealing temperature in the same range, respectively

treatment. In addition, the concerned thickness is increased for higher annealing temperature. In Fig. 6b, the Ga/(In + Ga) ratio roughly keeps as a constant along the depth direction, with a maximum variation of 0.02. However, compared the initial and stoichiometric composition of as-deposited CIGS to the samples annealed at lower temperatures (Fig. 5b), we may conclude that a Ga poor layer is formed at the film surface during annealing treatment. Results displayed in Fig. 6b allow us to assert that this Ga depletion area exhibits a thickness larger than 30 nm. In Fig. 6 c and d, the evolutions of Na and O atomic contents from the surface to the bulk of the CIGS film are displayed. A similar distribution, i.e. decrease from the surface to the bulk along depth direction, is observed in both cases. For annealing at 380 and 410 °C, the Na concentration is decreasing rapidly to zero at the region only 4 nm far from the surface. Whereas, after annealing at 450 °C, the Na signal is recorded far from the film surface and expands nearly on the 30 nm depth within the bulk. For annealing at 550 °C, the Na diffusion occurs far beyond 30 nm in depth, since our last recorded point gives an atomic percent close to 8 %. In the case of O content, a similar behavior, i.e. continuous decrease from the surface towards the bulk of the film, is recorded. After annealing at 380 °C, the initial O concentration at the CIGS film surface is only 2.5 % and decreases rapidly to zero along the depth direction. Higher annealing temperatures (450 and 550 °C) enhance O diffusion within the bulk. In the last case, for annealing temperature up to 550 °C, the O concentration at the film surface is close to 12 %, and remains 3 % at 30 nm in depth. Again, we may assert that the oxygen diffusion is occurring over more than 30 nm in depth when annealing CIGS film at 550 °C.

Based on the analyses of XPS, we may have some comment about the chemical composition evolutions neat the film surfaces versus annealing temperatures. When annealing from 380 to 550 °C, the Cu loss at the surface is enhanced and CIGS films are becoming Cu and Ga poor, but exhibiting a high concentration level of O and Na, in a good agreement with the phenomenon observed by Kronik et al. [25] in their co-evaporated CIGS films. At higher annealing temperature, more Se vacancies are created at the film surface, which might be occupied by the negatively charged O atoms coming from residual oxygen

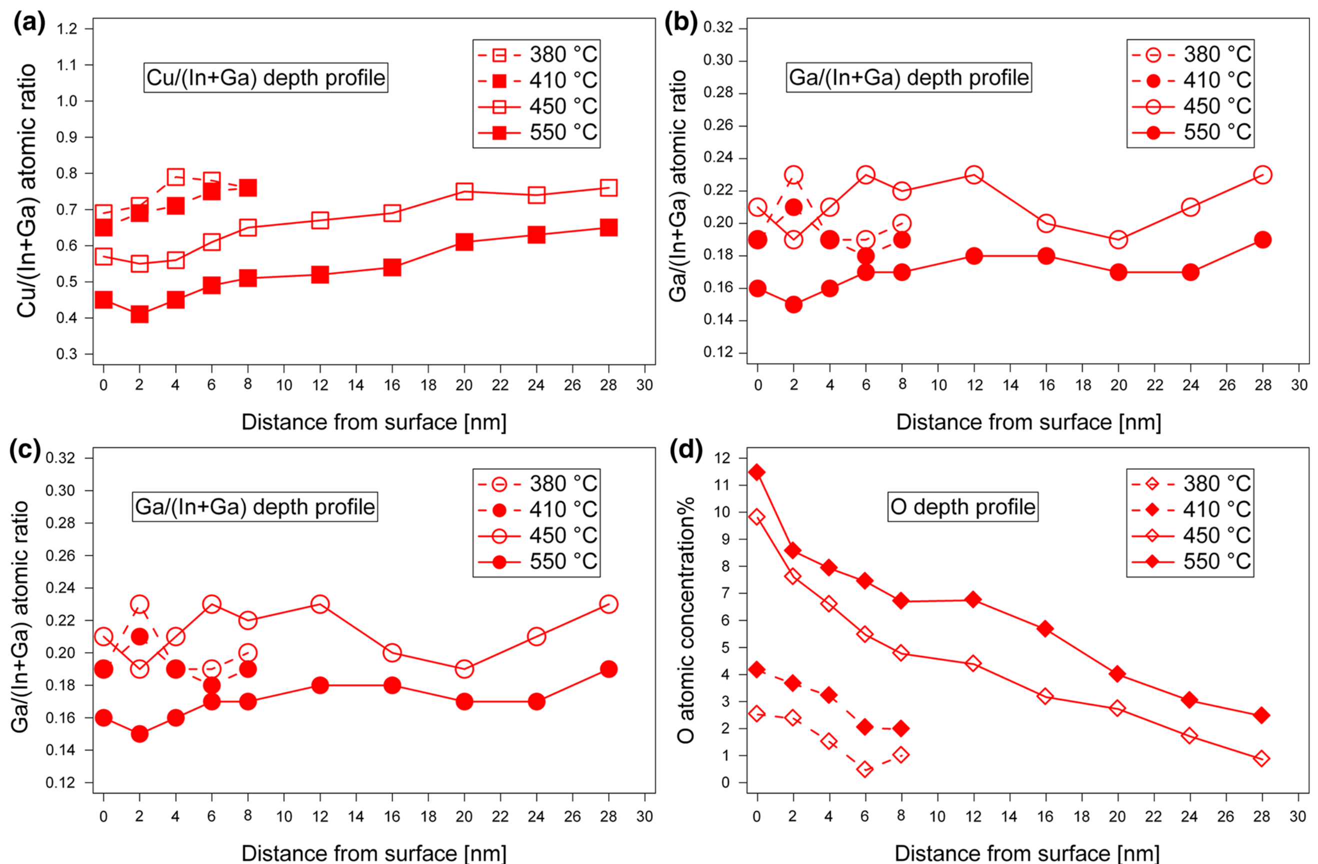

Fig. 6 Evolution of atomic ratios **a** Cu/(In + Ga) and **b** Ga/(In + Ga) obtained from XPS depth profiles of core levels analyses (Cu 2p, In 3d and Ga 2p) over the first 30 nm depth of CIGS films after annealing at 380, 410, 450 and 550 °C, and depth profiles of Na atomic content (**c**) and O atomic content (**d**) for the same annealing temperatures

within the furnace. As a result, In–O related compounds could be formed. Due to the large electron negativity difference between In and O atoms (1.7 and 3.5, respectively), In–O bonds exhibit a strong polar nature. On the contrary, covalent Cu-Se bonds are weaker. Therefore, Cu atoms are more positive and will be prone to leave initial surficial sites towards bulk, leading to a Cu poor surface area.

It should be pointed out that Na ions are originally in the SLG glass substrate. During the annealing treatment, it will diffuse into CIGS film and then, form some oxides. Theses oxides could enhance O absorption at the film surface as reported previously [26]. As a result, we can assume that the sodium has also corresponded to the Cu poor surface during annealing progress.

Since In atoms have a larger atomic radius than Ga atoms, the internal stress of CIGS film will be lowered by a preferential out diffusion of In relatively to Ga at the film surface during annealing [27]. As a result, for annealing above 380 °C, it is easier to form a single layer located at the CIGS film surface. This surface layer is Cu and Ga poor, with Na and O enrichment, as highlighted by the chemical and structural analyses presented in this study. However, previous works only reported such phenomenon in the CIGS film prepared by co-evaporation or selenization method. This work shows that the film prepared by sputtering a quaternary target has similar behaviours, which beyond our normal knowledge.

4 Conclusion

In this work, CIGS films were deposited by quaternary target sputtering and subsequent 30 min annealing in a Se-containing atmosphere at various temperatures. Between 240 and 270 °C, the surface covered by some Cu-Se compounds according to XRD, GIXRD and Raman analyses. XRD analyses evidenced some In_4Se_3 phase formed on CIGS film annealed at 240 °C. Therefore, we could assume that CIGS phase near the surface was split into CuSe, $CuSe_2$ and In_4Se_3 phases between 240 and 270 °C. A possible mechanism of such phase split was discussed in the paper. In addition, by calculating the evolution of FWHM values of (112) peak in CIGS phase ($Cu(In,Ga)Se_2$, JCPDS file 35-1102), we could conclude that the average

grain size increased with temperatures. On the other hand, the intensity of (204/220) peak became higher progressively from 310 to 550 °C. It indicated that the CIGS film formed a more random structure after annealing treatment compared with as-deposited film, which had a strong (112) texture. Above 380 °C, O and Na signals were observed on the film surface. Simultaneously, the surface became poor in Cu and Ga. With increased temperature, such region was expanded wider and wider. The strong relationship between Cu, Ga, O and Na compositions at CIGS surface was discussed in the paper.

Acknowledgments The first author acknowledges National Nature Science Foundation of China (51202227). A significant part of thin film characterization (GIXRD and XPS) was performed at the CNRS-IMN institute.

References

1. T. Nakada, Electron. Mater. Lett. **8**, 179–185 (2012)
2. S. Kang, R. Sharma, J.-K. Sim, C.-R. Lee, J. Alloys Compd. **563**, 207–215 (2013)
3. C.-K. Xu, H.-W. Zhang, J. Parry et al., Sol. Energy Mater. Sol. Cells **117**, 357–362 (2013)
4. P. Jackson, D. Hariskos, R. Wuerz, W. Wischmann, M. Powalla, Phys. Status Solidi RRL: Rapid Res. Lett. **8**, 219–222 (2014)
5. P. Guha, S.-N. Kundu, S. Chaudhuri, A.-K. Pal, Mater. Chem. Phys. **74**, 192–200 (2002)
6. J. Han, C. Liao, T. Jiang et al., Mater. Res. Bull. **49**, 187–192 (2014)
7. C.-P. Liu, C.-L. Chuang, Powder Technol. **229**, 78–83 (2012)
8. H.-S. Jadhav, R.-S. Kalubarme, S. Ahn et al., Appl. Surf. Sci. **268**, 391–396 (2013)
9. S. Furue, S. Ishizuka, A. Yamada, M. Iioka, H. Higuchi, H. Shibata, S. Niki, Sol. Energy Mater. Sol. Cells **119**, 163–168 (2013)
10. N.G. Dhere, Sol. Energy Mater. Sol. Cells **95**, 277–280 (2011)
11. H.F. Liang, U. Avachat, W. Liu, J. Van Duren, M. Le, Solid-State Electron. **76**, 95–100 (2012)
12. F.B. Dejene, Curr. Appl. Phys. **10**, 36–40 (2010)
13. J. Xiang, X. Huang, G. Lin et al., J. Electron. Mater. **43**, 2658–2666 (2014)
14. L. Ouyang, D. Zhuang, M. Zhao, N. Zhang, X. Li, L. Guo, R. Sun, M. Cao, Phys. Status Solidi (a) (2015). doi:10.1002/pssa.201532005
15. J. Liu, D. Zhuang et al., Vacuum **102**, 26–30 (2014)
16. Y.C. Lin, Z.Q. Lin, C.H. Shen et al., J. Mater. Sci. Mater. Electron. **23**, 493–500 (2012)
17. J. Liu, D. Zhuang, H. Luan et al., Prog. Nat. Sci. Mater. Int. **23**, 133–138 (2013)
18. G.-X. Liang, P. Fan, J.-R. Chi et al., J. Mater. Sci. Mater. Electron. **25**, 438–443 (2014)
19. J. Han, C. Liao, K. Zhao, M.-P. Besland, J. Cryst. Growth **382**, 56–60 (2013)
20. S. Roy, P. Guha, S.N. Kundu, H. Hanzawa et al., Mater. Chem. Phys. **73**, 24–30 (2002)
21. T. Mise, T. Nakada, Sol. Energy Mater. Sol. Cells **93**, 1000–1003 (2009)
22. A.R. Jeong, W. Jo, M. Song, S. Yoon, Mater. Chem. Phys. **134**, 1030–1035 (2012)
23. A. Gobeaut, L. Laffont, J.-M. Tarascon et al., Thin Solid Films **517**, 4436–4442 (2009)
24. J. Han, C. Liao, E. Gautron et al., Vacuum **105**, 46–51 (2014)
25. L. Kronik, U. Rau, J.-F. Guillemoles et al., Thin Solid Films **361–362**, 353–359 (2000)
26. D. Braunger, D. Hariskos, G. Bilger, et al. E-MRS Spring Meeting, Strasbourg (1999)
27. M. Marudachalam, R.W. Birkmire, H. Hichri, J. Appl. Phys. **82**, 2896–2905 (1997)